

Article

Not peer-reviewed version

A Miniaturized Thin-Film UWB Monopole Antenna Implemented with High-Dk Adhesive

[Duc Nguyen Dao](#) and [Jae-Young Chung](#)*

Posted Date: 19 July 2023

doi: 10.20944/preprints202307.1354.v1

Keywords: UWB; high-Dk adhesive; monopole antenna; thin film antenna



Preprints.org is a free multidiscipline platform providing preprint service that is dedicated to making early versions of research outputs permanently available and citable. Preprints posted at Preprints.org appear in Web of Science, Crossref, Google Scholar, Scilit, Europe PMC.

Copyright: This is an open access article distributed under the Creative Commons Attribution License which permits unrestricted use, distribution, and reproduction in any medium, provided the original work is properly cited.

Article

A Miniaturized Thin Film UWB Monopole Antenna Implemented with High-Dk Adhesive

Dao Duc Nguyen¹ and Jae-Young Chung^{2,*}

¹ Department of Electrical and Information Engineering, Seoul National University of Science and Technology, Nowon-gu, Seoul 01811, Korea; daonguyen3154@gmail.com

² Department of Electrical and Information Engineering, Seoul National University of Science and Technology, Nowon-gu, Seoul 01811, Korea

* Correspondence: jy chung@seoultech.ac.kr

Abstract: This paper presents the design of a miniaturized polyimide-based antenna for Ultra-Wideband (UWB) communication. Miniaturization is achieved through the utilization of adhesive material with a high dielectric constant (high-Dk). The goal of this work is to investigate the impact of such material on the antenna performance and to optimize its design for UWB operation. The manufacturing of the antenna using the proposed structure was developed and the prototype of antenna for UWB high-band (6 - 9 GHz) is measured and analyzed. By leveraging the high Dk of the adhesive material, the simulation and measurement results showed that the proposed antenna with high Dk adhesive film can achieve the compact dimension with good performance in gain, and time domain characteristics. The results of this study show a potential of exhibiting a reduction in the size of the antenna and will contribute to the advancement of miniaturized UWB antenna technology.

Keywords: UWB; high-Dk adhesive; monopole antenna; thin film antenna

1. Introduction

Ultra-Wideband (UWB) technology has increasingly aroused a lot of interest in many applications of high-speed wireless communication and accurate localization [1,2]. With the characteristic of wide bandwidth, UWB systems have the advantages of improvement in multi-path fading immunity, enhancement in ranging resolution, great ability of objective penetration, and large tolerance to interference with other wireless systems [2].

In UWB system, antenna is one of the most essential elements as it is responsible for transmitting and receiving signals. In the antenna design process for the UWB system, miniaturization is a challenge due to the physical size constraints imposed by their applications. In [3–5], antennas with monopole structure and Vivaldi structure are suggested for UWB systems. However, they have no flexible capabilities. On the other hand, the interest in research on flexible electronics has increased in response to the commercial trends in compact, portable, lightweight, and flexibility [6]. Several approaches for flexible printed circuit (FPC) antennas have been reported.

In [7], a tapered slot antenna using a 200 μm liquid crystal polymer (LCP) substrate is proposed. The design shows great radiation performance and excellent time-domain characteristics as very little distortion is introduced by the antenna. However, the bulky dimensions ($130 \times 66 \text{ mm}^2$) are not suitable for modern electronics integration. In [8], an elliptical-shaped monopole UWB antenna printed on Kapton polyimide substrate is presented. It shows good radiation characteristics and impedance matching, with low degradation when under bending effects. However, the size of it ($47 \times 33 \text{ mm}^2$) needs further miniaturized.

In [9], H. Bahrami et al. has designed flexible spiral-type dual-polarization antennas for neural recording systems by using a substrate of polyimide (PI) with a dielectric constant (Dk) of 3.5. In [10], a CPW-fed monopole with dimensions of $34.5 \times 26 \text{ mm}^2$ for wearable application is suggested. Polyester with $Dk = 3.2$ is used as an antenna substrate, and polydimethylsiloxane (PDMS) with $Dk = 2.3 - 2.8$ is used as an artificial magnetic conductor (AMC). In [11], Hong et al. proposed a design of

transparent and flexible antenna with ITO/Ag/ITO (IAI) multilayer for wearable glasses application. The PI film layer with $D_k = 3.5$ is chosen as the substrate. Phan et al. designed a microstrip monopole antenna "Sapin" covering the bandwidth from 2.2 - 10 GHz for wireless Local Area Network (WLAN) application [12]. The antenna dimension is $45 \times 28 \text{ mm}^2$ and the substrate is E4D paper with $D_k = 3.184$. In [13], an inverted-F structure with a bow-tie shape is suggested for wearable applications with the substrate consisting of two-layer PI with D_k of 3.5. Of all these works, low- D_k film materials are often chosen as the antenna's substrate because low- D_k material allows energy to be radiated out of the system, rather than being stored in the substrate, which results in increasing the bandwidth of resonance. However, to overcome the space limitation, one approach to miniaturization is to use a high- D_k substrate with the scarification of bandwidth.

Flexible Copper-Clad Laminate (FCCL) is usually used as the base material to create FPCs. FCCL consists layers of copper foil, PI film and bonding adhesive, providing the advantages such as high thermal stability and resistance to environmental factors [14]. Film material, however, usually has a low D_k . In the structure of a thin film antenna, the thickness of the bonding adhesive layer is comparable with the PI layer, therefore, its impact can be significant to the antenna's performance. Current technologies are focusing on making low dielectric constant (low- D_k) and low dielectric dissipation (low- D_f) adhesive bonding film for utilizing resonant bandwidth. To the best of the authors' knowledge, none of the existing research has investigated the effect of the adhesive layer on the performance of the antenna. Hence, for the first time, the utilization of a high- D_k bonding adhesive in the design and construction of the antenna is explored. By investigating the overall performance, valuable insights can be acquired to study the efficiency and potential of using high- D_k adhesive for thin film antennas. Besides the physical size constraint, other parameters must also be considered in the designing process of UWB antennas such as wide bandwidth, stable pattern characteristics, and good time-domain performance [15].

In this paper, we propose a design of antenna for UWB using a new adhesive material with high- D_k and low- D_f , showing that using such material could reduce the overall size of antenna while remaining the desired UWB characteristics. First, the antenna design for the high band of UWB (6 - 9 GHz) using high- D_k , low- D_f bonding sheet adhesive will be designed and parametric studies of important parameters are presented in Section 2. Next, the antenna fabrication and experimental results including radiation pattern, reflection coefficient, and gain are simulated and measured in Section 3. In Section 4, the time domain analysis is presented. Discussion and comparison with other existing flexible antennas will be presented and the final conclusion is stated in Section 5.

2. Design of thin film UWB monopole antenna

2.1. Thin film layer stack up

The target operation frequency range of the proposed thin film UWB antenna is 6 - 9 GHz which is the UWB high-band for indoor UWB transmissions when no mitigation techniques are used [16]. Among a variety of UWB antenna structures, a bell shape monopole antenna was chosen as shown in Figure 1 since this structure is compatible with thin films, and offers broadband impedance matching and omnidirectional radiations [17–19]. The stack up of the thin film is also depicted in Figure 1. It consists of top and bottom copper layers deposited on PI layers. These a pair of copper/PI layer is bonded together by the middle adhesive layer which exhibits a high D_k property in this proposed design. The D_k and D_f of the PI layer is 3.3 and 0.005, respectively, while the D_k and D_f of the adhesive layer is 6 and 0.006. The thicknesses of copper, PI and adhesive layers are $12 \mu\text{m}$, $50 \mu\text{m}$ and $50 \mu\text{m}$. The total thickness of the antenna combination is $174 \mu\text{m}$. It is worth noting that the thickness of one layer of copper and adhesive is the same while the D_k of adhesive layer is 1.8 times higher than PI. Thus, the high D_k property of the adhesive layer is supposed to promote thin film antenna miniaturization similar to previous reports on PCB antenna miniaturization using high D_k substrates [20–22].

2.2. Simulation results

Figure 1 shows the geometry of the proposed printed monopole antenna backed by a partial ground plane, where W_0 and L_0 are the width and length of the antenna, respectively. The dimension of the proposed antenna is $20 \times 12 \text{ mm}^2$. The ground of the antenna is designed based half elliptical shape with the vertex length of L_g and AR is the aspect ratio of the ellipse, which is the ratio between the length of the major axis and the minor axis. The radiator patch is determined by the width of W_0 and the length of the patch is a combination of a straight line with a length of L_1 and a curve which is drawn by using the spline function. L_f and W_f are the length and width of the transmission line. A small rectangular with the width of W_s is placed at the starting point of the feed line for soldering with a SubMiniature version A (SMA) connector. Table 1 shows the list of these parameters and their optimized value.

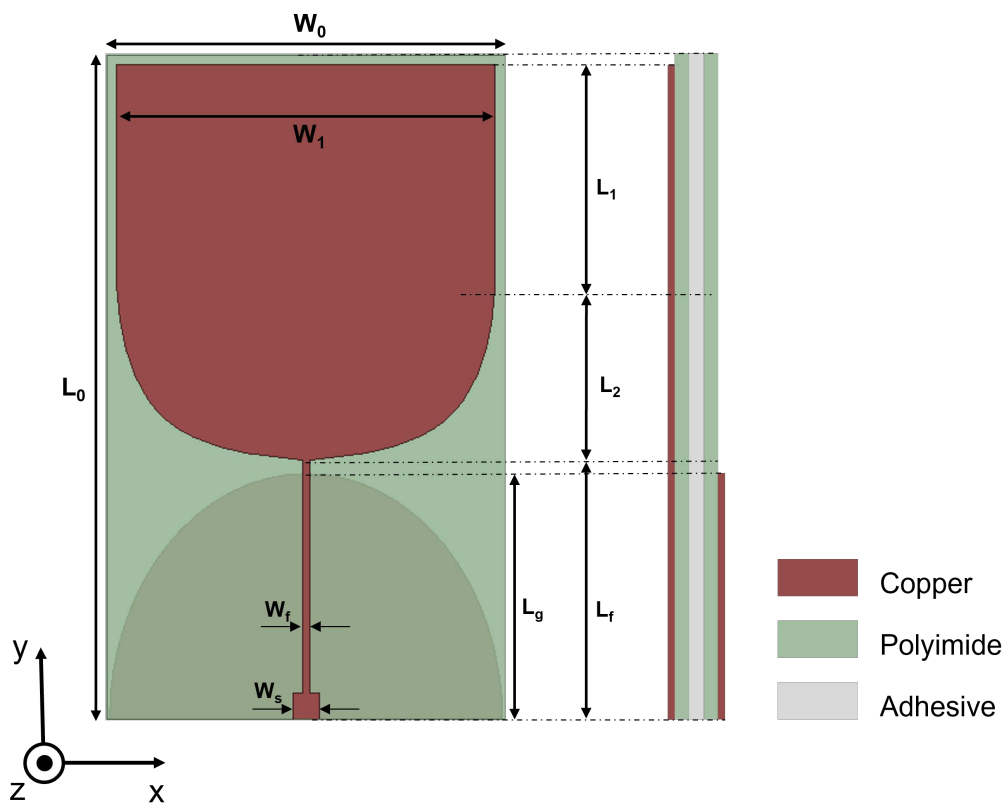


Figure 1. Geometry of the proposed thin film UWB monopole antenna.

Table 1. Optimized parameters of proposed high band antenna.

Symbol	Value	Symbol	Value
W_0	12.0 mm	L_f	7.8 mm
L_0	20.0 mm	W_f	0.2 mm
W_1	11.4 mm	L_g	7.4 mm
L_1	6.7 mm	W_s	0.8 mm
L_2	5.2 mm	AR	1.25

Figure 2 presents the simulation results of the S_{11} of the antenna while changing some key parameters in the designing process. The S_{11} refers to the reflection coefficient of the antenna and indicates the amount of power that is reflected back toward the source when an electromagnetic signal is transmitted through the antenna. To improve the impedance and radiation properties, a partial

ground is designed. The effects of length L_g are analyzed as in Figure 2a. As we can see, the smaller ground plane's length will result in poor impedance matching results and with the longer ground plane's length, the resonant frequency will shift to a lower frequency. It is worth noting that the increase in the ground plane's length will result in a smaller gap between the antenna's patch and the ground. With L_g of 7.7 mm, this gap is so small that the bandwidth gets narrower. Only the ground length L_g of 7.3 mm meets the required $S_{11} < -10$ dB over an interested frequency bandwidth of 6 - 9 GHz. Hence, 7.3 mm is chosen as the value of L_g .

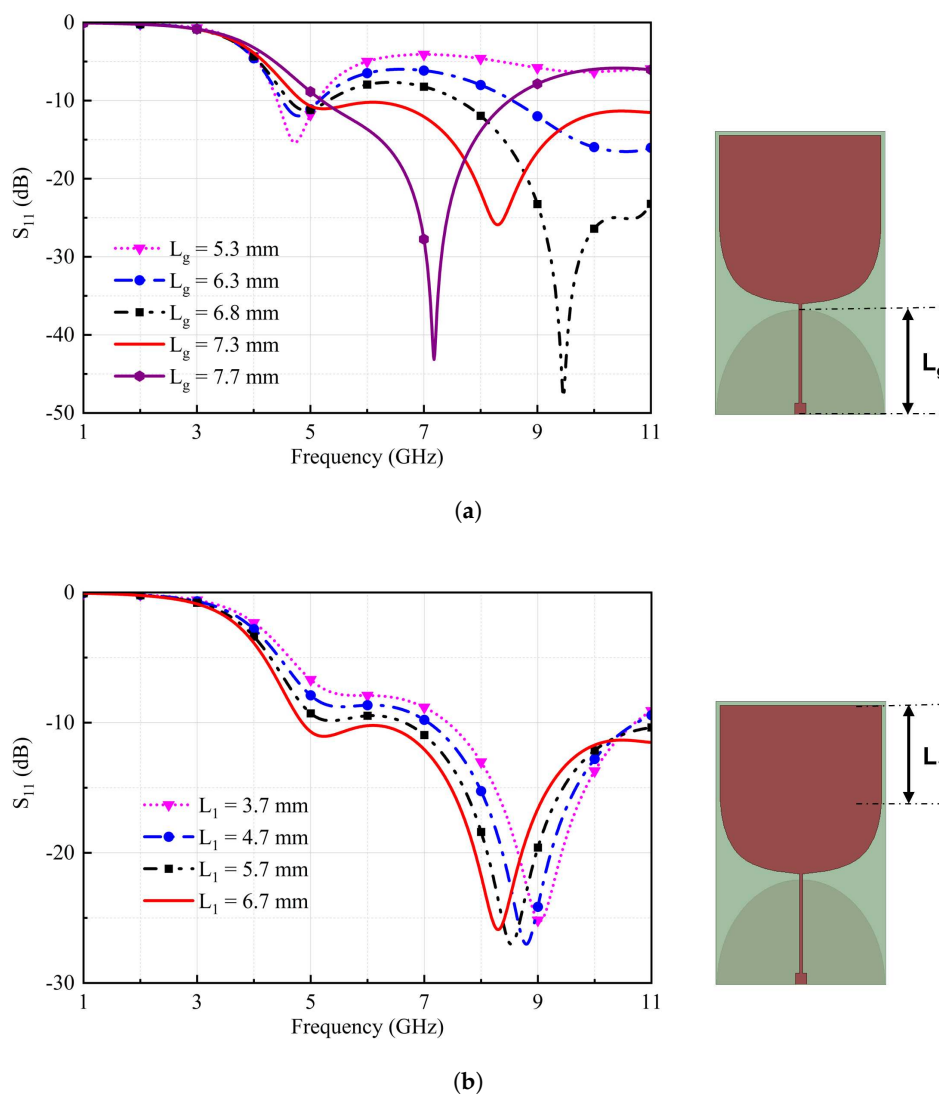


Figure 2. Simulation results of S_{11} versus frequency by varying (a) L_g , (b) L_1 .

Figure 2b shows how the length of the straight patch L_1 influences the magnitude of reflection coefficient S_{11} over frequency. As can be seen, when the patch gets longer, resonant frequency tends to move towards the lower band. This can be explained that the longer patch length results in a longer electrical length and the propagation occurs in a longer wavelength, meaning the lower resonant frequency. Moreover, the $S_{11} > -10$ dB around the mid-band of UWB is recorded in shorter patch length. On the other hand, with L_1 of 6.7 mm, a good $S_{11} < -10$ dB is provided for our interested frequency band 6 - 9 GHz. For this reason, the appropriated L_1 value is chosen as 6.7 mm. To verify the theoretical results, the following section will address this with experiments.

3. Antenna fabrication and measurements

A photograph of the fabricated antenna with the front and back view is shown in Figure 3. For experimental measurement, our antenna requires connection to a Vector Network Analyzer (VNA) via a connector. The part number of the SMA connector used is Board Edge SMA SM06FS006 of Withwave company. Its operating frequency is from 10 MHz to 26.5 GHz with 50Ω matched. From Figure 4, we can notice some agreements of reflection coefficient S_{11} between the simulation and measurement. Both the simulated and measured results have a bandwidth of more than 6 - 9 GHz for $S_{11} < -10$ dB, which is satisfied our target frequency band for the high band of UWB. The measurement impedance bandwidth is recorded from 5 - 10.8 GHz. The discrepancy in simulation and measurement results is from the widened ground effect due to the SMA connector, which is neglected in the simulation environment.

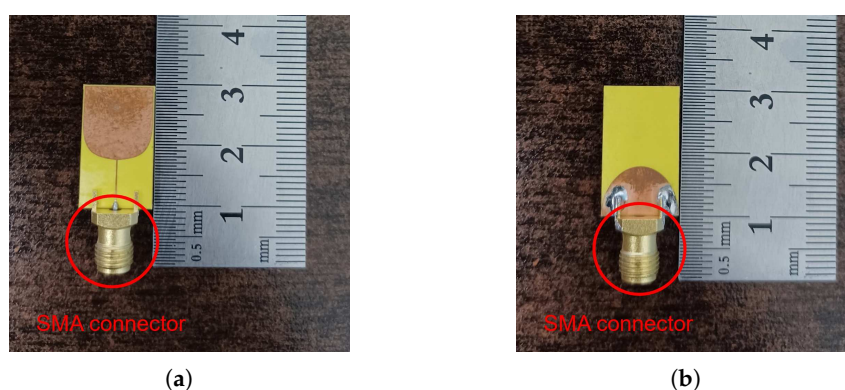


Figure 3. Fabricated antenna prototype with an SMA connector (a) Front view, (b) Back view.

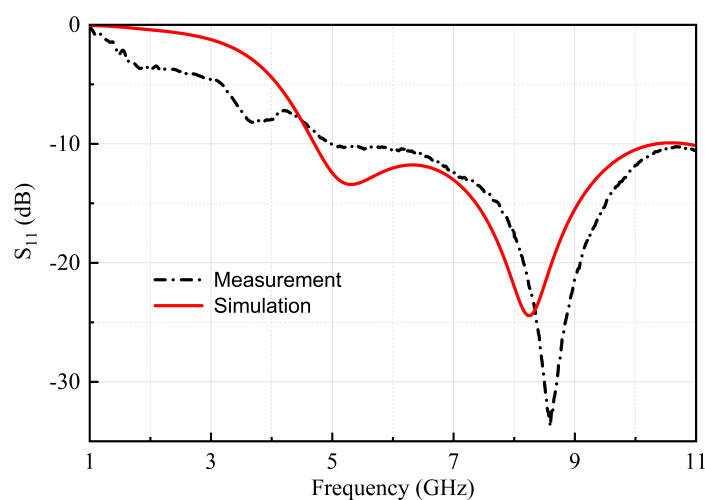


Figure 4. Comparison of S_{11} simulation and measurement results.

For the far-field gain experiment, the antenna measurement was done in an anechoic chamber. Figure 5 shows the picture of the fabricated antenna in the chamber while doing measurements. Figure 6 shows the comparison between simulation and measurement results in terms of normalized radiation patterns in the H-plane, which is the XY-plane ($\theta = 90^\circ$), and E-plane, which is the XZ-plane ($\phi = 0^\circ$) of the designed antenna operating at the frequency of 6 GHz and 7.5 GHz. Apparently, the omnidirectional radiation pattern in the E-plane (XZ-plane) and the form of figure-eight shape in the H-plane (XY-plane) are provided. It is worth noting that the measurement results do include the effect of cable and connector, which impacts results.

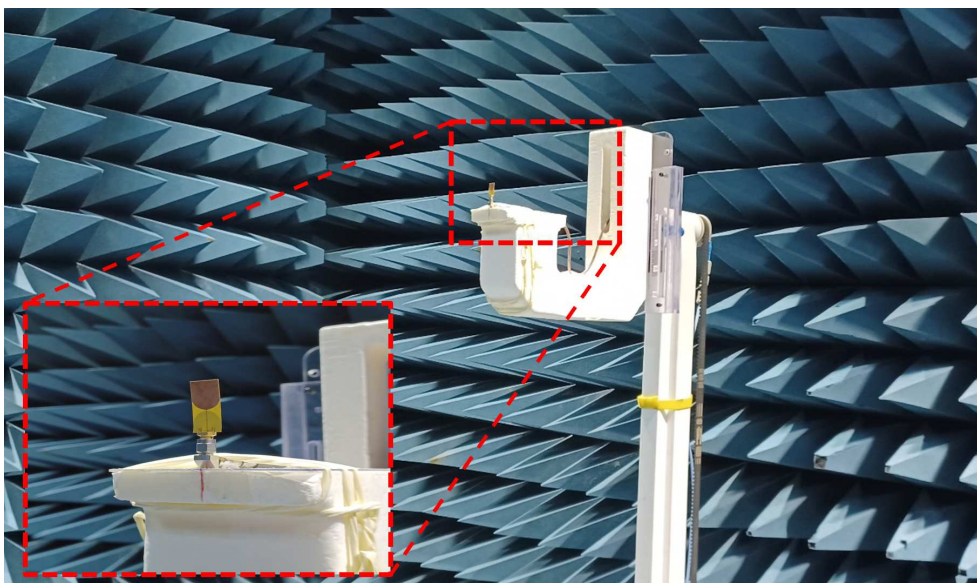


Figure 5. The fabricated antenna located in anechoic chamber.

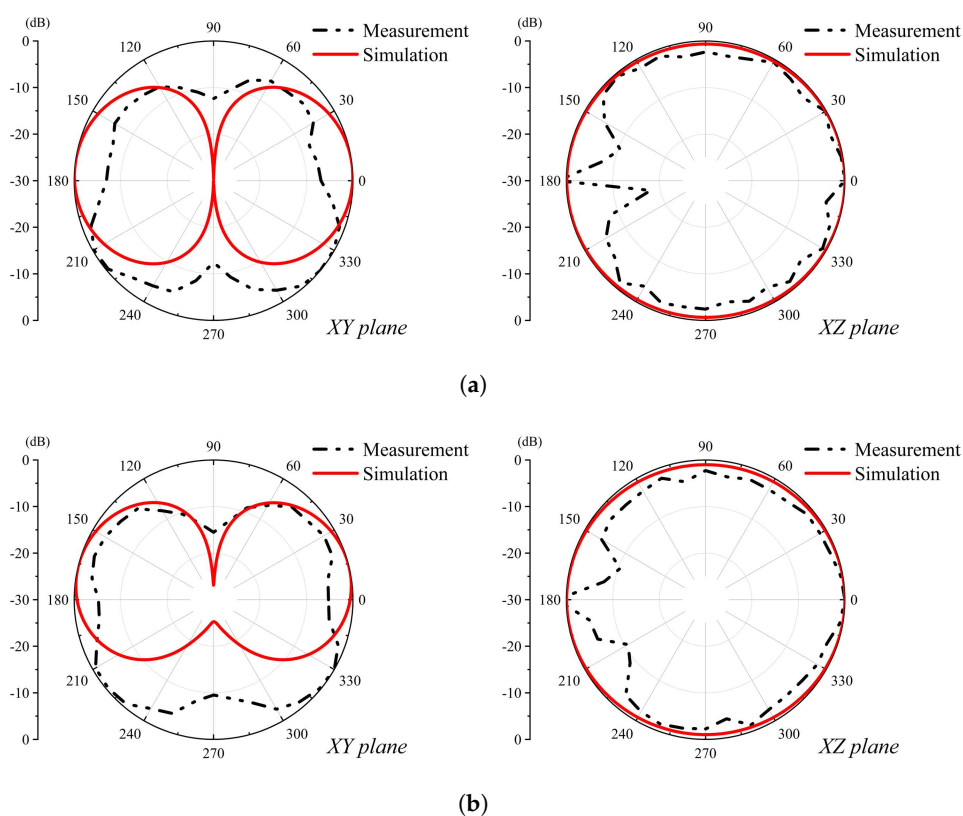


Figure 6. Comparison of simulated and measured normalized radiation patterns at (a) 6 GHz, (b) 7.5 GHz.

Figure 7 shows the peak gain of the fabricated antenna in simulation and experiment in XZ-plane ($\phi = 0^\circ$). The measured gain has a very similar trend to the simulated gain. However, it is lower than that in simulation, this can be explained by the loss of cable, connector and the chamber is not calibrated effectively. The average measured peak gain is about 2.1 dB over the frequency band, and the maximum peak gain of 2.8 dB is measured at 8 GHz, which is 3.6 dB in the simulation. The antenna

gain is acceptable for an omnidirectional radiated antenna. The measurement results in the time domain of the proposed antenna will be discussed in the following section.

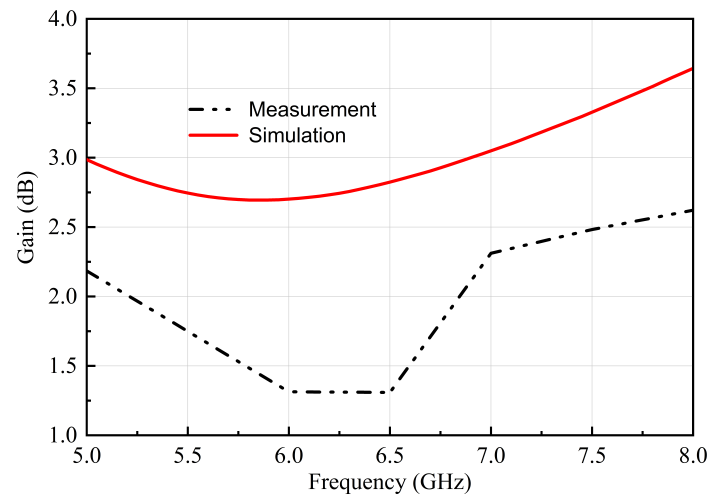


Figure 7. Comparison of peak realized gain measurement and simulation at $\phi = 90^\circ$.

4. Time domain analysis

This section will analyze the pulse-shape preservation capabilities of the antenna. In the ideal case, the received UWB pulse should have the same shape as the transmitted pulse. Therefore, the antenna design process should consider this to minimize the distortion effects produced by the antenna itself and the environment.

To analyze the time domain performance, the common approach is to consider the antenna as a linear time-invariant (LTI) system described by its transfer function $H(\omega)$ or transmission parameter S_{21} [23–25]. The S_{21} measurement with a VNA is set up inside an anechoic chamber. For setting up the time domain analysis, the two identical prototypes of proposed antenna are arranged at a distance of 100 mm. Figure 8 shows three distinct configurations for time domain measurement: side by side, face by face, and face by side. The time domain measurement setup is shown in Figure 9.

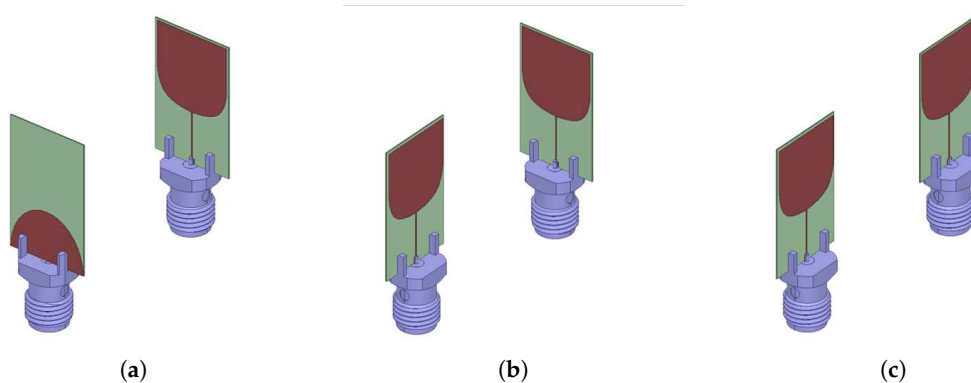


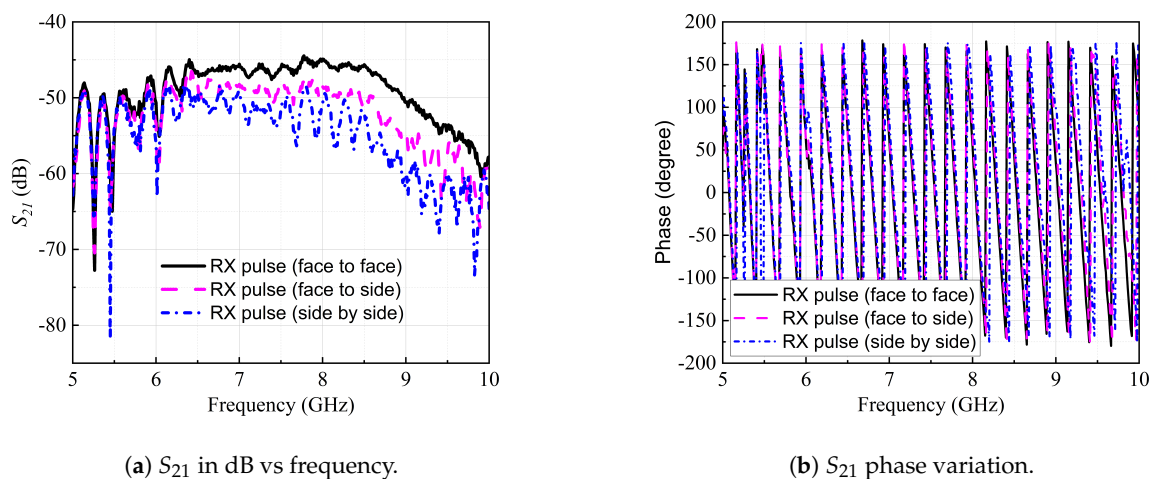
Figure 8. Time domain measurement configurations (a) Face to face, (b) Face to side, (c) Side by side.

The system transfer functions of the antenna systems S_{21} of two identical antennas will be presented and analyzed. In order to transmit pulses without any distortion, the system transfer function should be constant over the desired frequency. By plotting S_{21} both magnitude and phase, we can quantify the pulse distortion effects based on their linearity characteristics. Figure 10 shows the measured magnitude and phase results of S_{21} for three configurations. It can be observed that

the magnitude is quite stable and the phase response is linear over the frequency range of 6 - 9 GHz, which signifies that the pulse shape is preserved without any out-of-phase components.



Figure 9. Time domain measurement setup.



(a) S_{21} in dB vs frequency.

(b) S_{21} phase variation.

Figure 10. Measured S_{21} of three configurations.

For analyzing the pulse shape preservation capability of the antennas, the Square-Root Raised Cosine Signal (SRRC) pulse is chosen as the input pulse for its bell-shaped energy distribution across frequency range [26]. The mathematical form of the SRRC pulse is shown in (1):

$$F_{SSRC}(t) = \left[\frac{2\beta}{\pi\sqrt{T_S}} \times \frac{\cos \left[(1 + \beta)\pi \frac{t}{T_S} \right] + \frac{\sin \left[(1 - \beta)\pi \frac{t}{T_S} \right]}{4\beta \frac{t}{T_S}}}{\left[1 - \left(4\beta \frac{t}{T_S} \right)^2 \right]} \right] \quad (1)$$

where β is the roll-off factor for bandwidth control, t is the time, and $T_S = 1/R_S$, R_S is the symbol rate.

Figure 11 shows the amplitude-modulated SRRC pulse and its power spectrum density corresponding with the UWB indoor spectrum mask. The roll-off factor and the symbol rate of the modulated SRRC pulse are 0.4 and 10 GHz, respectively. The center frequency of the input pulse is chosen as 7.5 GHz, with the bandwidth covering the high band of UWB 6 - 9 GHz.

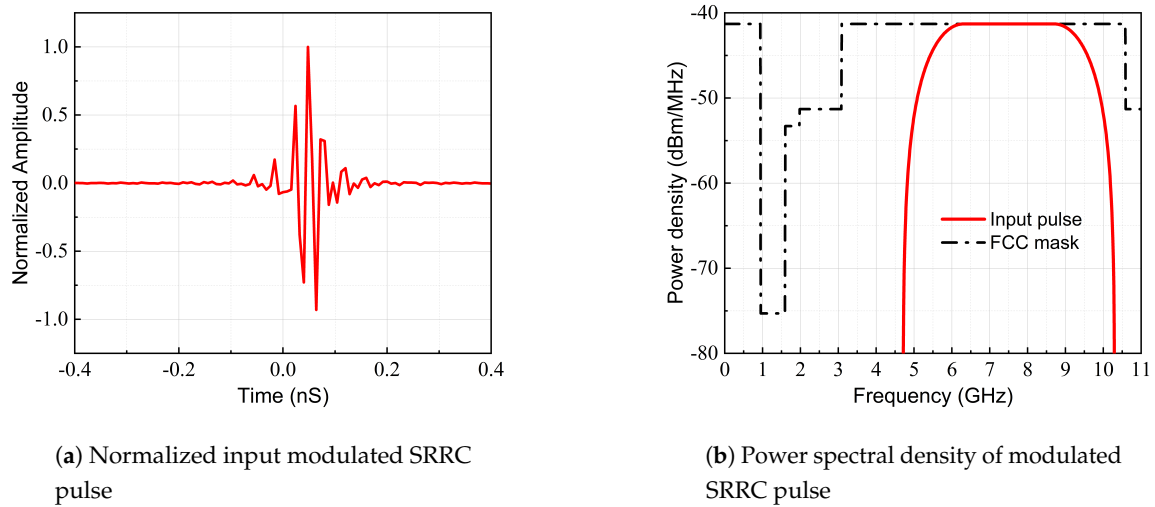


Figure 11. Simulated input modulated SRRC pulse.

Figure 12 represents the pulse shape comparison of the modulated SRRC input pulse and received pulses in three configurations. The received signals are calculated by multiplying the original input signal with the transfer function in the frequency domain and then applying an inverse Fourier transform to get them back to the time domain. The received signals in the three configurations are almost identical, showing the consistency of the pulse preservation capability of proposed antennas in the omnidirectional plane of antennas.

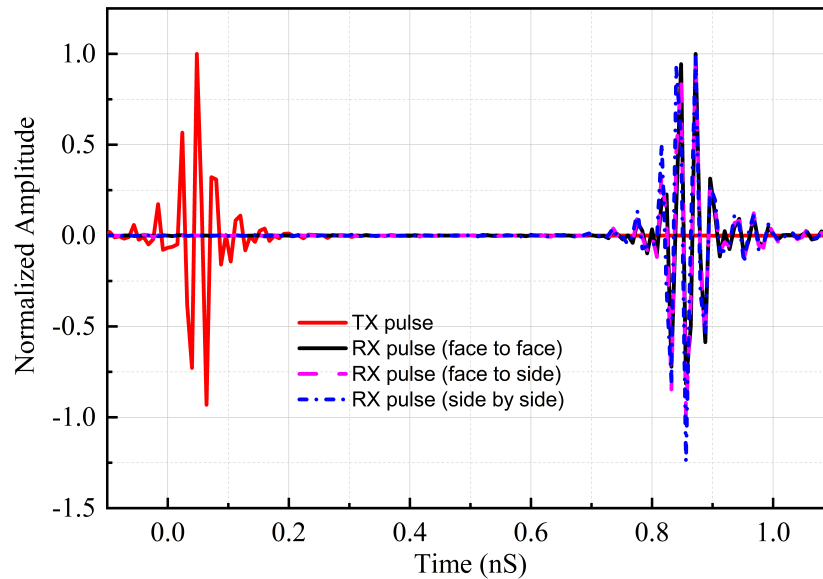


Figure 12. Simulated normalized amplitude of input and received signal pulse.

To further investigate the equivalence between the transmitted and received waveform, the fidelity factor can be calculated as (2):

$$F = \max_{\tau} \left[\frac{\int_{-\infty}^{+\infty} s(t)s_r(t + \tau)dt}{\int_{-\infty}^{+\infty} |s(t)|^2 dt \int_{-\infty}^{+\infty} |s_r(t + \tau)|^2 dt} \right] \quad (2)$$

where $s(t)$ and $s_r(t)$ are two signals to be compared. The fidelity factor is done by taking the cross-correlation between 2 normalized signals when they are overlapped [27,28]. A fidelity factor of 1 means that the transmitted pulse and the received pulse are identical, there is no distortion during transmission. Meanwhile, the fidelity factor equals 0 indicating that the two signals are completely different. Table 2 shows the fidelity factor of antennas of three configurations. The results show that the fidelity is greater than 0.85, validating that the proposed antenna does not distort the signal pulse significantly.

Table 2. Fidelity factor of three configurations.

	Face to face	Face to side	Side by side
Fidelity factor	0.904	0.919	0.853

The group delay shows the time delay of specific frequency components when traveling through a device. If the signal only contains one frequency component, which is a perfect sine-wave, the whole signal would experience a stable group delay. The UWB antenna; however, consists of numerous frequency components. In order to avoid being delayed differently at different frequencies, a linear phase response is required. This means a stable group delay over frequency is mandatory in UWB systems to satisfy the ideal case of pulse reservation condition [29].

In simple terms, group delay τ_{group} is the rate of change of phase shift with respect to frequency. It delay can be expressed mathematically as the negative derivative of phase response ϕ with respect to frequency ω :

$$\tau_{\text{group}} = -\frac{d\phi}{d\omega} \quad (3)$$

The measured group delay is presented in Figure 13. We can recognize a quite stable group delay in three configurations at desired frequency band. Hence, the proposed antenna has been determined to be suitable for UWB communications.

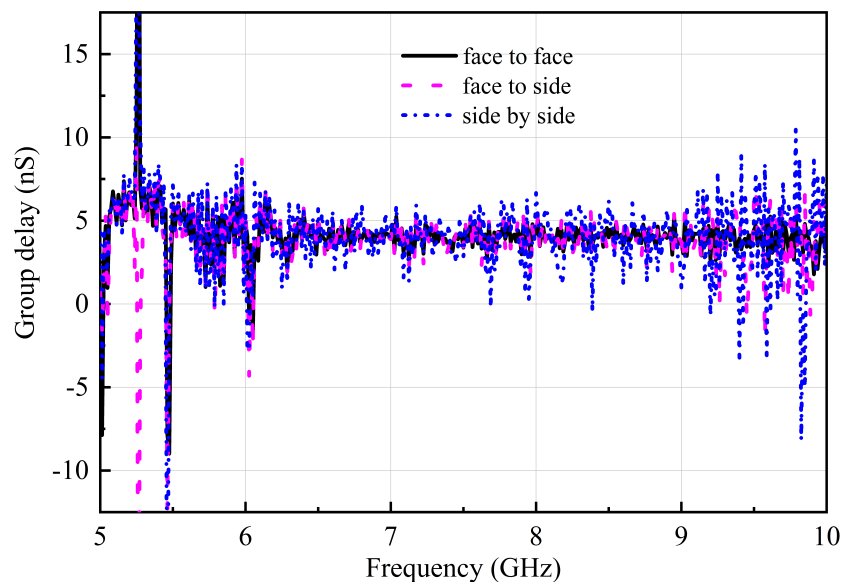


Figure 13. Measured group delay of three configurations.

5. Conclusions

The proposed antenna is compared with other existing flexible antennas in Table 3. Both absolute size and electrical size are presented, showing that the proposed antenna has a relatively compact dimension with a very thin thickness and the proposed antenna can operate with the bandwidth to

cover the UWB high band. The free space wavelength λ_0 is chosen with respect to the lower frequency of the frequency band. The maximum gain is lower than some works due to the trade-off with a smaller size, but it is acceptable for such a monopole antenna with omnidirectional radiation patterns.

Table 3. Comparison of various existing flexible antennas with the proposed antenna.

Ref	Absolute size (mm^3)	Electrical size (λ_0^3)	Operating frequency (GHz)	Max gain (dB)
[30]	$28.1 \times 17.1 \times 1.4$	$0.47 \times 0.29 \times 0.023$	5 - 14	N/A
[31]	$25 \times 10 \times 1.6$	$0.25 \times 0.1 \times 0.016$	3 - 11.2	1.5
[32]	$20 \times 20 \times 1$	$0.35 \times 0.35 \times 0.017$	5.2 - 6.86	2.94
[33]	$31 \times 38 \times 0.135$	$0.39 \times 0.48 \times 0.0017$	3.8 - 4.5	3.1
[34]	$32 \times 38 \times 0.118$	$0.59 \times 0.69 \times 0.0022$	5.5 - 7	N/A
[35]	$14 \times 18 \times 1$	$0.14 \times 0.18 \times 0.01$	2.94 - 11.17	3.6
[36]	$47 \times 25 \times 0.14$	$0.48 \times 0.25 \times 0.0014$	3.04 - 10.7	N/A
[37]	$32 \times 52 \times 0.28$	$0.43 \times 0.69 \times 0.0037$	4 - 8	4.1
This work	$20 \times 12 \times 0.174$	$0.33 \times 0.2 \times 0.0025$	5 - 10.8	2.9

To summarize, in this paper, a miniaturized antenna thin film antenna using a new high-Dk adhesive material is designed and fabricated for UWB communication. The antenna features a compact dimension of $20 \times 12 \text{ mm}^2$ with the thickness of $174 \mu\text{m}$ and exhibits a wide impedance bandwidth covering from 5 - 10.8 GHz. The experimental results closely align with the simulations, demonstrating excellent agreement. Additionally, the proposed antenna demonstrates favorable time-domain performance. This work gains insights into achieving the thin film compact antennas by manipulating the adhesive layer's characteristics.

Funding: This work was supported in part by Basic Science Research Program through NRF funded by the Ministry of Education (NRF-2019R1A6A1A03032119) and in part by the Technology development Program (S3238198) funded by the Ministry of SMEs and Startups (MSS, Korea).

Conflicts of Interest: The authors declare no conflict of interest.

References

1. Elsanhoury, M.; Mäkelä, P.; Koljonen, J.; Välisuo, P.; Shamsuzzoha, A.; Mantere, T.; Elmusrati, M.; Kuusniemi, H. Precision Positioning for Smart Logistics Using Ultra-Wideband Technology-Based Indoor Navigation: A Review. *IEEE Access* **2022**, *10*, 44413–44445.
2. Zafari, F.; Gkelias, A.; Leung, K.K. A Survey of Indoor Localization Systems and Technologies. *IEEE Communications Surveys & Tutorials* **2019**, *21*, 2568–2599.
3. Jeon Gwang-Hun, Dzagbletey Philip Ayiku, C.J.Y. A Cross-Joint Vivaldi Antenna Pair for Dual-Pol and Broadband Testing Capabilities. *J. Electromagn. Eng. Sci* **2021**, *21*, 201–209.
4. Mekki Kawther, Necibi Omrane, L.S.G.A. A UHF/UWB Monopole Antenna Design Process Integrated in an RFID Reader Board. *J. Electromagn. Eng. Sci* **2022**, *22*, 479–487.
5. Bala Susmita, Reddy P. Soni, M.R.S.P.P.S.S. Printed Monopole Antenna with Tree-Like Radiating Patch and Flower Vase-Shaped Modified Ground Plane Useful for Wideband Applications. *J. Electromagn. Eng. Sci* **2022**, *22*, 256–264.
6. Haider R. Khaleel and Hussain M. Al-Rizzo and Daniel G. Rucker. Compact polyimide-based antennas for flexible displays. *J. Display Technol.* **2012**, *8*, 91–97.
7. Nikolaou, S.; Ponchak, G.; Papapolymerou, J.; Tentzeris, M. Conformal double exponentially tapered slot antenna (DE TSA) on LCP for UWB applications. *IEEE Trans. Antennas Propag.* **2006**, *54*, 1663–1669.
8. HR, K.; HM, A.R.; Rucker DG, M.S. A compact polyimide-based UWB antenna for flexible electronics. *IEEE Antennas Wirel Propag Lett.* **2012**, *11*, 564–567.
9. Bahrami, H.; Mirbozorgi, S.A.; Ameli, R.; Rusch, L.A.; Gosselin, B. Flexible, polarizationdiverse UWB antennas for implantable neural recording systems. *IEEE Trans. on Biom. Ckts and Sys.* **2016**, *10*, 38–48.
10. F, W.; Arslan, T. A wearable ultra-wideband monopole antenna with flexible artificial magnetic conductor. *2016 Loughborough Antennas & Propagation Conference (LAPC)* **2016**.

11. S., H.; Kang, S.H.; Jung, C.W. Transparent and flexible antenna for wearable glasses applications. *IEEE Transactions on Antennas and Propagation* **2016**, *64*, 2797–2804.
12. P., P.H.; Vuong, T.P.; Benech, P.X.; Borel, P.; Delattre, A. Printed flexible wideband microstrip antenna for wireless applications. *International Conference on Advanced Technologies for Communications (ATC)* **2016**, pp. 12–14.
13. LJ, X.; H, W.; Y, C.; Y, B. A flexible UWB inverted-F antenna for wearable application. *Microw Opt Technol Lett.* **2017**, *59*, 2514–2518.
14. Hwang, S.M.; Lim, J.H.; Lee, C.M.; Park, E.C.; Choi, J.H.; Joo, J.; Lee, H.J.; Jung, S.B. Fabrication of two-layer flexible copper clad laminate by electroless-Cu plating on surface modified polyimide. *Transactions of Nonferrous Metals Society of China* **2009**, *19*, 970–974.
15. P., P.H.; Vuong, T.P.; Benech, P.; Xavier, P.; Borel, P.; Delattre, A. On the dispersive properties of the conical spiral antenna and its use for pulsed radiation. *IEEE Transactions on Antennas and Propagation* **2003**, *51*, 1426–1433.
16. Niemelä, V.; Haapola, J.; Hämäläinen, M.; Iinatti, J. An Ultra Wideband Survey: Global Regulations and Impulse Radio Research Based on Standards. *IEEE Communications Surveys & Tutorials* **2017**, *19*, 874–890.
17. Allen, B.; Dohler, M.; Okon, E.; Malik, W.; Brown, A.; Edwards, D. *Ultra-wideband : antennas and propagation for communications, radar and imaging*; John Wiley & Sons, Ltd, 2007.
18. Matin, M. *Ultra Wideband Communications*; IntechOpen: Rijeka, 2011.
19. G.M., G.T.; M.A., P.S.; H, J.A. *Ultra Wideband Antennas: Design, Methodologies, and Performance*; CRC Press: Boca Raton, 2016.
20. Hoorfar, A.; Perrotta, A. An experimental study of microstrip antennas on very high permittivity ceramic substrates and very small ground planes. *IEEE Transactions on Antennas and Propagation* **2001**, *49*, 838–840.
21. Ding, C.; Luk, K.M. Low-Profile Planar Dielectric Polarizer Using High-Dielectric-Constant Material and Anisotropic Antireflection Layers. *IEEE Transactions on Antennas and Propagation* **2021**, *69*, 8494–8502.
22. Lee, B.; Harackiewicz, F. Miniature microstrip antenna with a partially filled high-permittivity substrate. *IEEE Transactions on Antennas and Propagation* **2002**, *50*, 1160–1162.
23. Zwierzchowski, S.; Jazayeri, P. Derivation and determination of the antenna transfer function for use in ultra-wideband communications analysis. *Wireless Proc* **2003**, pp. 157–161.
24. Mohammadian, A.; Rajkotia, A.; Soliman, S. Characterization of UWB transmit-receive antenna system. *IEEE Conference on Ultra Wideband Systems and Technologies*, 2003, pp. 157–161.
25. Chen, Z.N.; Wu, X.H.; Li, H.F.; Yang, N.; Chia, M. Considerations for source pulses and antennas in UWB radio systems. *IEEE Transactions on Antennas and Propagation* **2004**, *52*, 1739–1748.
26. Zhang, X.; Larson, L.E.; Asbeck, P.M. *Design of Linear RF Outphasing Power Amplifiers*; Norwood, MA: Artech House: London, 2003.
27. Lamensdorf, D.; Susman, L. Baseband-pulse-antenna techniques. *IEEE Antennas and Propagation Magazine* **1994**, *36*, 20–30.
28. Quintero, G.; Zurcher, J.F.; Skrivervik, A.K. System Fidelity Factor: A New Method for Comparing UWB Antennas. *IEEE Transactions on Antennas and Propagation* **2011**, *59*, 2502–2512.
29. Kwon, D.H. Effect of antenna gain and group delay variations on pulse-preserving capabilities of ultrawideband antennas. *IEEE Transactions on Antennas and Propagation* **2006**, *54*, 2208–2215.
30. Saha, T.K.; Goodbody, C.; Karacolak, T.; Sekhar, P.K. A compact monopole antenna for ultra-wideband applications. *Microwave and Optical Technology Letters* **2019**, *61*, 182–186.
31. Chahat, N.; Zhadobov, M.; Sauleau, R.; Ito, K. A Compact UWB Antenna for On-Body Applications. *IEEE Transactions on Antennas and Propagation* **2011**, *59*, 1123–1131.
32. Babu, B.A.; Madhav, B.; Vineel, B.; Chandini, G.; Amrutha, C.; Rao, M. Design and Analysis of a Circularly polarized flexible, compact and transparent antenna for Vehicular Communication Applications. *Journal of Physics: Conference Series* **2021**, *1804*, 012192.
33. Hossain, A.R.; Karacolak, T. CPW-Fed Compact Circularly Polarized Flexible Antenna for C Band Applications. 2023 United States National Committee of URSI National Radio Science Meeting (USNC-URSI NRSM), 2023, pp. 246–247.
34. Venkateswara Rao, M.; Madhav, B.T.P.; Anilkumar, T.; Prudhvinaadh, B. Circularly polarized flexible antenna on liquid crystal polymer substrate material with metamaterial loading. *Microwave and Optical Technology Letters* **2020**, *62*, 866–874.

35. Naser-Moghadasi, M.; Sadeghzadeh, R.A.; Sedghi, T.; Aribi, T.; Virdee, B.S. UWB CPW-Fed Fractal Patch Antenna With Band-Notched Function Employing Folded T-Shaped Element. *IEEE Antennas and Wireless Propagation Letters* **2013**, *12*, 504–507.
36. Kirtania, S.G.; Younes, B.A.; Hossain, A.R.; Karacolak, T.; Sekhar, P.K. CPW-Fed Flexible Ultra-Wideband Antenna for IoT Applications. *Micromachines* **2021**, *12*.
37. Fang, R.; Song, R.; Zhao, X.; Wang, Z.; Qian, W.; He, D. Compact and Low-Profile UWB Antenna Based on Graphene-Assembled Films for Wearable Applications. *Sensors* **2020**, *20*.

Disclaimer/Publisher's Note: The statements, opinions and data contained in all publications are solely those of the individual author(s) and contributor(s) and not of MDPI and/or the editor(s). MDPI and/or the editor(s) disclaim responsibility for any injury to people or property resulting from any ideas, methods, instructions or products referred to in the content.